Optical Strain Gauge-Based on a Hetero-Core Fiber Macro-Bending Sensor

Hiroshi Yamazaki and Kazuhiro Watanabe

***Abstract*—This paper describes a novel approach for optical strain sensing based on a hetero-core fiber optic macro-bending sensor. A gauge substrate for the proposed sensor was designed to transduce the tensile and compression strain by changing to a gentle bending curvature on the fiber; thus, the hetero-core fiber detects the strain on the substrate as the transmitted light lost. Because optical fibers perform as a flexible structure in a buckling scheme owing to their slenderness, the mechanical properties of the proposed sensor can be widely tuned by the shape and mechanical properties of the gauge substrate. Experiments demonstrated that the proposed strain gauge with a spring-structured substrate made of SUS304 showed a strain applied within ±3100 $\mu\epsilon$ with a sensitivity of up to -9.14×10^{-4} dB/ $\mu\epsilon$, and responded to temperature changes from 0 °C to 60 °C with -1.10×10^{-2} dB/°C owing to the thermal expansion of the substrate. Furthermore, both the strain and temperature sensitivities are tunable by changing the geometrical parameters of the gauge substrate.**

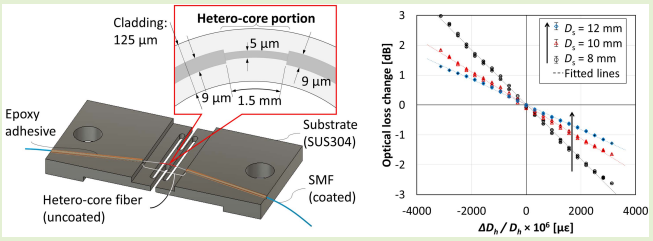

***Index Terms*— Fiber optic sensor, strain gauge, structural health monitoring, hetero-core.**

I. Introduction

STRUCTURAL Health Monitoring (SHM) is an emerging, attractive diagnostic tool to assess the safety of civil infrastructures and machines by quantifying the health of structures from the eigenfrequency, the magnitude of deformation, physical damage, and corrosion [1], [2]. The most attractive feature of SHM systems is that the structural status can be quantitatively evaluated by sensor data without empirical judgment by inspection workers. SHM systems include data acquisition and transmission modules, signal processing, data storage, and system identification based on the measured data [3], [4]. In particular, because sensors are utilized to monitor primary information of target structures, they are crucial components whose accuracy has a considerable influence on the total performance of SHM systems.

Most SHM systems have employed strain sensors, force sensors, accelerometers, and displacement sensors based on piezoelectric transducers, strain gauges, and capacitive sensors. Although these electronic sensor components have been a mainstream of sensing technologies for decades in fault diagnosis of structures, they are susceptible to electromagnetic wave interference (EMI), temperature changes from day and night, electrical shorts due to water invasion, and metal corrosion when the system is operated for a long term in an outdoor environment.

However, optical fiber sensors are promising techniques with outstanding features over these electronic sensors, because they are lightweight, robust against corrosion, immune to EMI, have a low transmission loss, have multiplex capabilities, and have a sensing element implanted during construction [5], [6]. For instance, fiber Bragg gratings (FBG) are the most frequently used fiber sensors for strain and temperature measurements of structures [7]–[10]. FBG sensors consist of Bragg gratings in a fiber core which transduce the variation of grating periods due to strain and temperature into the wavelength of reflected light called Bragg wavelength. Other fiber optic sensors have been also developed for strain measurements based on, for example, Mach-Zehnder interferometry [11]–[13], Fabry-Perot interferometry [14], modal interferometry [15]–[18], and long-period fiber grating [19]. However, despite their high sensitivities to strain, and distributed or multi-point sensing availability, these fiber sensors require a complicated optical interrogator to measure a highly precise peak shift. Moreover, they are restricted in terms of measurement range by the elastic limit of silica fibers, and

Manuscript received June 12, 2020; accepted June 13, 2020. Date of publication June 26, 2020; date of current version October 16, 2020. This work was supported by the JSPS KAKENHI under Grant 18K11363 and Grant 19K14930. The associate editor coordinating the review of this article and approving it for publication was Dr. Carlos Marques. *(Corresponding author: Hiroshi Yamazaki.)*

Hiroshi Yamazaki is with the Department of Information Systems Sciences, Faculty of Science and Engineering, Soka University, Tokyo 192-8577, Japan (e-mail: hyamazaki@soka.ac.jp).

Kazuhiro Watanabe is with the Department of Science and Engineering for Sustainable Innovation, Faculty of Science and Engineering, Soka University, Tokyo 192-8577, Japan (e-mail: kazuhiro@soka.ac.jp).

Digital Object Identifier 10.1109/JSEN.2020.3005139

need to correct the difference between strain measured by a sensing fiber and that on host materials due to the existences of fiber coating and adhesive layers [5]. To tackle this issue, polymer optical fibers [20]–[23] have several mechanical advantages over silica fibers including a lower Young's modulus and a higher elastic limit, whereas their higher thermo-optic coefficients, humidity cross-sensitivity due to moisture absorption, and the viscosity of composing polymers can harm their strain sensing performances during use in harsh environments [22], [24].

Compared to conventional fiber optic sensors, a hetero-core fiber optic sensor has been reported as an intensity-modulated macro-bending sensor composed of two single-mode fibers with different cores [25]. This sensor has been experimentally confirmed to have a bending loss that is sensitive to a gentle curvature radius of several tens of millimeters and thus could result in a cost-effective and power-saving measurement scheme by means of a light-emitting diode (LED) and a photodiode (PD) [26], [27]. It has thus far been demonstrated that this sensor can measure displacement on the order of several millimeters with a displacement-to-bending converter mechanism [28]. In this configuration, a hetero-core fiber is mounted on a pair of fiber clampers by which the hetero-core portion is placed at the center, and the fiber is bent based on Euler's buckling by changing the distance between the clampers. According to Euler's buckling theory [29], the slender column structure of the fiber is regarded as a flexible structure in the case of contraction because the buckling stress is much lower than the tensile stress. Additionally, the change in the curvature of fiber can be enlarged by shortening the initial distance between the clampers, which possibly will result in the enhancement of the displacement sensitivity. Therefore, the hetero-core fiber optic sensor is capable of a minute displacement measurement over a short distance between fiber clampers with less restriction on the mechanical properties of the fiber materials; additionally, it does not require a pre-tension like FBG or other fibers for installation on host structures.

In this study, we proposed a novel optical strain gauge that uses a hetero-core fiber macro-bending sensor. The hetero-core fiber optic strain gauge (HCF-SG) consists of a hetero-core fiber mounted on a spring-structured substrate. In this structure, the spring part mainly deforms when the substrate is stressed, and the change in fiber curvature is subjected to the deformation of the spring; thus, the HCF-SG transduces the applied strain into an optical loss change in the hetero-core fiber. The sensitivity and the measurement range of the sensor were determined by the rate of curvature change to the applied strain and the limitation of the allowable curvature of the fiber; this can be modified by the initial distance between two fixed points on the hetero-core fiber on the substrate. In a series of experiments, the HCF-SG was confirmed to have a sensitivity to the applied strain of approximately 10^{-4} dB/$\mu\epsilon$ with sufficient linearity and precision, and it could detect strain changes on an aluminum plate, which was in good agreement with a commercial electrical resistance strain gauge. Additionally, it was demonstrated that the HCF-SG had a temperature dependency that was mainly caused by the thermal expansion of the substrate, which could be tuned by the geometry of the substrate.

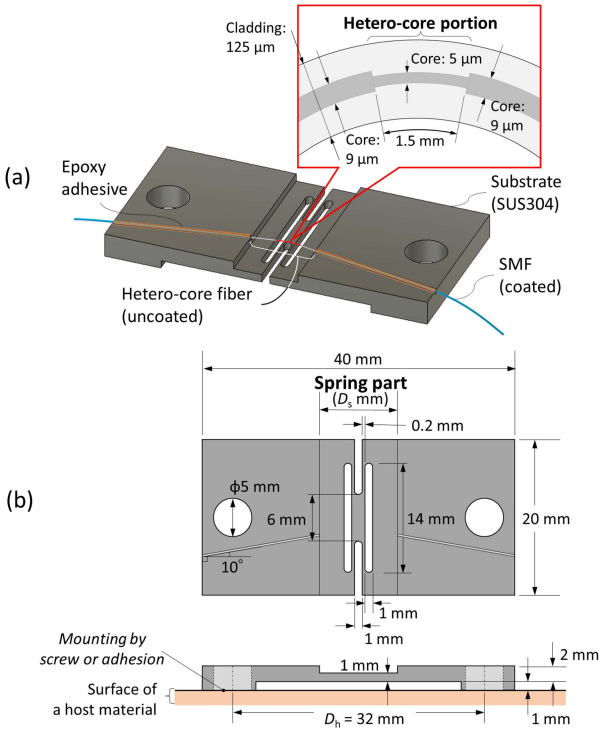

Fig. 1. Structure of a hetero-core fiber optic strain gauge (HCF-SG): (a) Appearance of the sensor and (b) a diagram of the gauge substrate.

II. Sensor Principle

A. HCF-SG Structure

Figure 1 shows a schematic drawing of the proposed HCF-SG. This sensor is composed of a substrate made of SUS304 austenite stainless steel and an optical fiber centered at the hetero-core portion mounted by epoxy adhesive. SUS304 is a representative steel that is superior in formability and has the ability to deform without fracturing; thus, it can be stretched without brittle fracture when forming a spring structure. The hetero-core optical fiber was fabricated by inserting and fusion splicing a single-mode fiber (SMF) segment with a small core diameter of 5 μm in a SMF transmission line with a 9-μm core diameter. The spliced SMF segment is called the hetero-core portion, at which the transmitted light on the 9-μm-core SMF line is partially propagated to a cladding layer owing to the mismatch with the transmission mode of the 5-μm-core SMF. Previously, it was verified that the optical loss on the hetero-core portion increased monotonically with an increase in curvature of the hetero-core portion, and it had a high linearity for displacement with a displacement-to-bending converter mechanism. Considering the trade-off relation between the linearity and the sensitivity of the hetero-core fiber discussed in the literature [28], the hetero-core portion was set to be 1.5 mm in length.

As shown in Fig. 1(b), the gauge substrate contains a spring part between the two mounting points of the hetero-core fiber to convert the strain on the host material to a macro-bending change on the hetero-core fiber. The top surface of the spring

part is scraped by 1 mm for the fiber line attached on the substrate to cross above it with no contact. At fiber mounting positions on the left and right sides of the substrate, linear channels are machined on the upper surface to guide the fiber line, making an angle of 10 degrees from the longitudinal direction of the substrate to predetermine the bending direction of a hetero-core fiber between the channels. Furthermore, the hetero-core fiber gets an initial curve by stretching the substrate while the fiber is being attached for preventing the fiber from stretching taut for a tensile strain. Additionally, the protective layer on the hetero-core fiber is first removed from the region crossing over the spring part in order not to disturb the rapid deformation of the bare fiber due to the very low plasticity of glass fiber.

On the bottom of the substrate, two short legs with 1-mm heights are on the left and right sides for attaching to a host structure by fastening with screws or adhering. When the host structure is stressed, the substrate transfers the total displacement on the host material between two attachment points to the deformation of the spring part. Therefore, the change in the length of the spring part, which is represented by ΔD_s, is expressed as

$$\Delta D_s = \tilde{\varepsilon_h} D_h, \tag{1}$$

where $\tilde{\varepsilon_h}$ and D_h represent the given strain and the initial interval between the attachment points, respectively. Considering the linear response of the hetero-core fiber to the displacement reported in the literature [28], the optical loss of the hetero-core fiber can be expressed as

$$l = \beta \Delta D_s, \tag{2}$$

where l represents the optical loss of the hetero-core fiber, and β is the sensitivity to the displacement, depending on the initial length of the fiber beam, which is almost equivalent to D_s. From Eqs. (1) and (2), it was found that the optical loss of the hetero-core fiber on the substrate linearly depends on the average strain applied between the attachment points on the host material.

B. Strain Sensitivity of the HCF-SG

To evaluate the strain sensitivity of the HCF-SG, a static strain measurement test was performed as shown in Fig. 2. In this experiment, the sensor was fastened by screws with a distance of $D_h = 32$ mm on a fixed stage and a linear motorized stage to obtain the tensile and compression strain by the motorized stage. When the motorized stage was displaced by ΔD_h, the effective strain for the tested sensors can be represented as $\Delta D_h / D_h$, which is hereafter described as positive in the tensile direction. An LED/PD measuring instrument with a center wavelength of 1.31 μm was connected to the fiber transmission line to monitor the change in the transmitted light intensity. Moreover, because the bending behavior of the hetero-core fiber to the strain is affected by D_s and the length of the spring part is almost equivalent to the fiber beam length, three sensor samples with $D_s = 8$, 10, and 12 mm were tested to investigate how D_s depends on the strain sensitivity.

Figure 3(a) shows the optical loss changes when applying strain to the HCF-SGs over ten trials within ± 3100 $\mu\epsilon$ with a

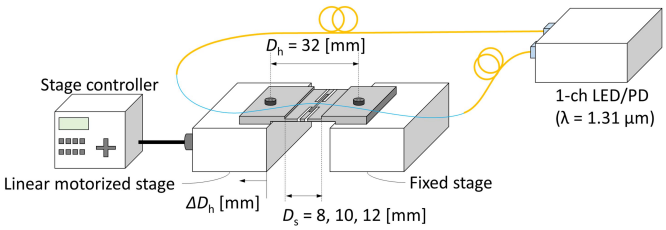

Fig. 2. Experimental setup for the static strain measurement using the proposed HCF-SGs.

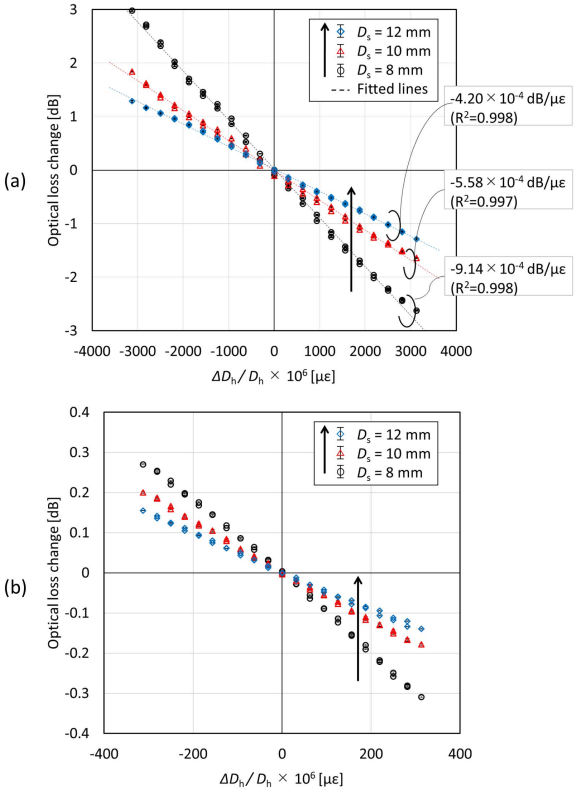

Fig. 3. Optical loss variations of the proposed HCF-SGs as a function of tensile and compression strain under the following conditions: (a) range of -3100 to 3100 $\mu\epsilon$ with a step of 310 $\mu\epsilon$, and (b) the narrow range of -310 to 310 $\mu\epsilon$ with a step of 31 $\mu\epsilon$, where the plots indicate the average values for ten trials and the error bars indicate the standard deviations.

step of 310 $\mu\epsilon$. The optical loss linearly varied with the strain in both directions of tensile and compression in which the linear regression of the measured data and linear fitting lines yielded a correlation coefficient (R^2) of over 0.996. The linear responses of the HCF-SGs are reasonable because the hetero-core fiber has a linear sensitivity to displacement according to the displacement-to-bending converter mechanism [28]. Moreover, upon comparing the strain coefficients approximated by the linear regression for the three sensors, it was found that the shorter the D_s becomes, the more the strain sensitivity increases. Apparently, the curvature of the fiber beam buckling for a certain displacement increases with a decrease in beam length, which is because of the increment of sensitivity with the shortened D_s. Considering Eqs. (1) and (2), the strain

sensitivity of the HCF-SG can be described as

$$l = \beta D_h(\Delta D_s/D_h) = \alpha_{str}\tilde{\varepsilon_h}, \tag{3}$$

where α_{str} represents the strain coefficient of the HCF-SG. Because $\Delta D_s/D_h$ in this experiment can be regarded as $\tilde{\varepsilon_h}$, Eq. (3) can be rearranged as

$$\alpha_{str} = \beta D_h. \tag{4}$$

Moreover, the hetero-core fiber functions unless the fiber is fractured by excess bending, and the SUS304 gauge substrate has enough toughness not to be fractured within the strain range. Hence, the full range of bending loss on the hetero-core fiber predominately determines the limit of the measurement range. In a preliminary test, we confirmed that the hetero-core fiber can endure (with a linear response) at least the curvature corresponding to the bending loss of 6 dB, which is obvious from Fig. 3(a) for the case of $D_s = 8$ mm. Therefore, there is a trade-off between the strain sensitivity and the measurement range, which can cover the range of $\pm$ 3280, $\pm$5380, and $\pm$7140 $\mu\epsilon$ for the cases of $D_s = 8$, 10, and 12 mm, respectively.

Furthermore, when applying a strain with a minimal step of 31 $\mu\epsilon$ for the motorized stage to the HCF-SGs within $\pm$310 $\mu\epsilon$ for ten times, the sensors maintained the linearity of the optical loss responses to the applied strain, as shown in Fig. 3(b). The values of the standard deviation for each step, which are drawn as error bars, are negligibly small in Fig. 3(b) and were less than 2.42×10^{-3}, 3.83×10^{-3}, 1.12×10^{-3} dB for $D_s = 8$, 10, and 12 mm, respectively, which is equivalent to 2.72, 4.19, and 1.23 $\mu\epsilon$ upon considering each strain coefficient. Thus, these results indicate that the developed HCF-SG measures both tensile and compression strain with a high linearity and high precision with $\mu\epsilon$-order strains, in addition to not requiring a pre-tension like FBG or other conventional fiber optic strain sensors. Moreover, they are tunable for the sensitivity and measurement range simply by modifying the combination of D_s and D_h.

III. Strain Monitoring on a Host Material

To discuss the strain detectability for stressed structures, the performance of the HCF-SG was investigated when mounting on an aluminum (Al) base plate to which tensile stress was given. Figure. 4(a) shows the schematics of an HCF-SG mounted on an Al base plate with the dimensions of $2\text{mm}^{\text{t}} \times 20\ \text{mm}^{\text{w}} \times 120\ \text{mm}^{\text{l}}$, which was screwed to a fixed stage and a motorized stage with a distance of 100 mm. The HCF-SG was attached using a cyanoacrylate adhesive at the center position spaced by 50 mm from the fixed end combined with an electric resistance strain gauge (ER-SG) as a reference at a point spaced by 20 mm from the fixed end. To confirm how the sensor response varies on a host structure from the characteristics shown in Fig. 3, we employed the HCF-SG sample with $D_s = 8$ mm tested in Section II B. Figure 4(b) shows the configuration of the stage control and data acquisition system, with which tension was given to the base plate by the motor-driven stage using the two following trapezoidal stress patterns: (a) 10 pulses with rise and fall times of 1.0 s and a time period of 3 s and (b) 10 pulses with rise and fall times of 0.5 s and a time period of 5 s. The responses of the HCF-SG and the ER-SG were simultaneously monitored at a sampling rate of 50 Hz.

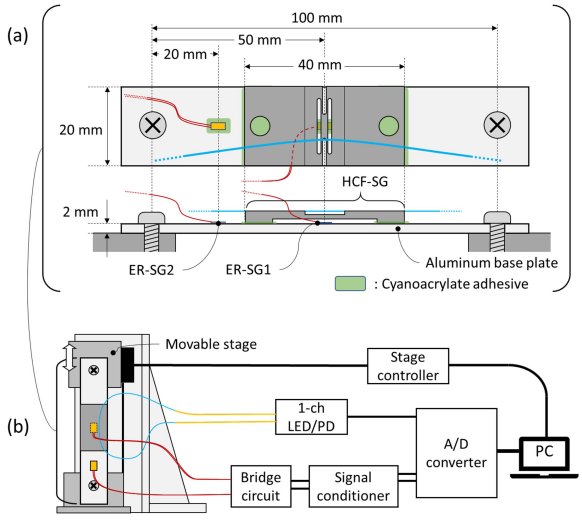

Fig. 4. Experimental setup for the strain measurement on an aluminum base plate using the developed HCF-SG and electric resistive strain gauges (ER-SG1 and ER-SG2) as references: (a) schematics of the sensors on the plate and (b) diagram of the control and measurement system.

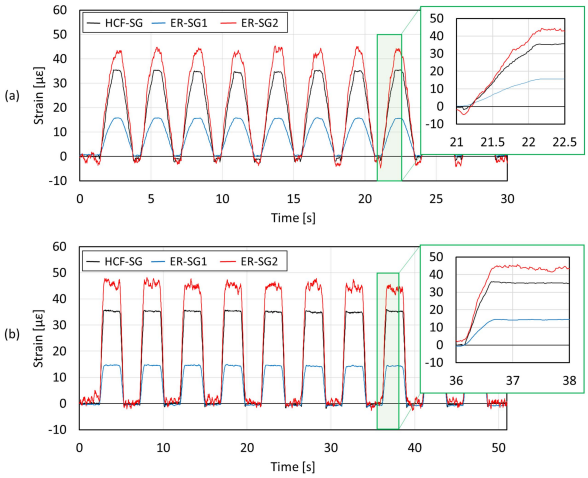

Fig. 5. Temporal profiles of the HCF-SG (black line), ER-SG1 (blue line), and ER-SG2 (red lines) on an Al base plate for two trapezoidal stress patterns under the following conditions: (a) 10 pulses with rise and fall times of 1.0 s and a time period of 3 s and (b) 10 pulses with rise and fall times of 0.5 s and a time period of 5 s.

Figure 5 shows the temporal changes in strain data measured by the HCF-SG and the ER-SGs when applying two trapezoidal stress patterns. The plotted data for the HCF-SG were calculated from the obtained loss changes by the strain coefficient (α_{str}) in Section II B. As shown in both Figs. 5(a) and (b), the periodic waveforms for the HCF-SG were in good agreement with the waveforms of the ER-SG1 and ER-SG2, except for the amplitudes. The differences in the amplitudes among the three sensors may have occurred because the strain distribution in the entire system, including

TABLE I
PHYSICAL PARAMETERS OF THE COMPONENTS FOR FE ANALYSIS

Structure	Material	Young's modulus [GPa]	Poisson ratio	Vol. mass density [kg/m^3]
Gauge substrate	SUS304	192	0.29	8930
Base plate	Aluminum	70	0.30	2700

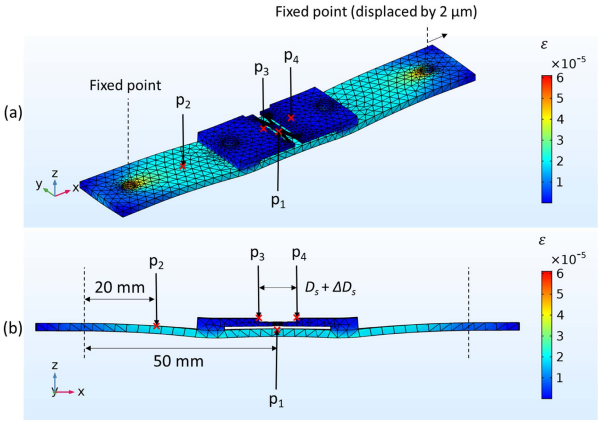

Fig. 6. FE analysis results of the HCF-SG substrate mounted on an Al plate under the condition of a tension applied between two fixed points of the Al plate in the x-axis direction with a 2-μm displacement; (a) external view and (b) side view from the y-direction. The surface plot shows the maximum principal strain. In this case the default D_S was set to 8 mm.

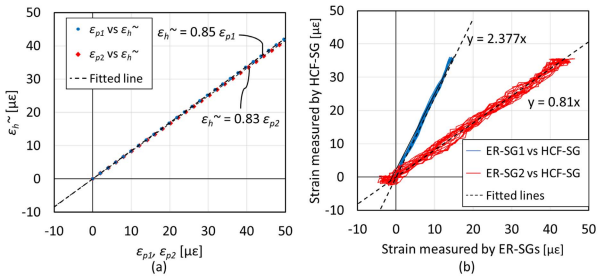

Fig. 7. Comparison between the FE analysis and experimental results for the ER-SGs and HCF-SG; (a) $\tilde{\varepsilon_h}$, ε_{p1}, and ε_{p2} represent the strain observed by the HCF-SG and the principal strains at p_1 p_2 where ER-SGs were mounted, respectively, and (b) the strain data measured by the HCF-SG and the ER-SGs, as shown in Fig. 5(a).

in the Al plate and the gauge substrate, was biased due to the strain transfer mechanism at the interfaces between the Al plate, the substrate, and the hetero-core fiber.

For further analysis of the strain transfer mechanism between the host structure and the HCF-SG, the strain distribution was simulated by finite element (FE) analysis using COMSOL Multiphysics. The model simply consists of an Al plate and a SUS304 gauge substrate with the same forms as shown in Fig. 4(a) except for the fiber beam line, this is because the flexibility of the fiber beam is much higher than those of other components so that the mechanical effect on the total system would be negligible. Young's modulus, Poisson's ratio, and the volumetric mass density of each component are listed in Table I. The two interfaces between the Al plate and the gauge substrate were assumed to be perfectly fixed.

Fig. 6 shows the shape and strain distribution map when the Al plate was stretched by 2 μm at two screw fixed points in the x-axis direction, where the deformation scale was enhanced by 3000 times. The color map indicates the amount of maximum principal strain on each mesh element. The principal strain almost uniformly distributed over the Al plate except for in the vicinities of the fixed points and two interfaces between the Al plate and the gauge substrate. This was because the substrate deforms at the spring part with such a low strain on each mesh element that the stress negligibly transmits on the substrate between the interfaces. Nevertheless, the Al plate and the gauge substrate are locally curved in the vicinities of the interfaces; this occurs because the strain on the upper surface of the Al plate is restricted by the stiffness of the substrate material.

To compare the FE analysis with the experimental results, we calculated three specific values from the FE simulation results, including the ε_{p1} and ε_{p2}, the principal strains at locations p_1 and p_2 where ER-SG1 and ER-SG2 were mounted, respectively, and the distance between p_3 and p_4, representing the length of the spring part, $D_s + \Delta D_s$, when a tension was applied to the Al plate by 5 μ m in displacement. From Eq. 1, a strain detected by the HCF-SG can be estimated as $\tilde{\varepsilon_h} = \Delta D_s / D_h$. Figures 7(a) and (b) show the FE simulation result for $\tilde{\varepsilon_h}$, ε_{p1}, and ε_{p2} and the experimental result from Fig. 5(a), respectively. As shown from Fig. 7(a), $\tilde{\varepsilon_h}$ increases linearly to ε_{p1} and ε_{p2} with almost equivalent values. As shown in Fig. 7(b), the output of HCF-SG also is linear to those of ER-SG1 and ER-SG2 with a same order of ratios as in the FE simulation, whereas there was a difference between the ratios possibly because of the adhesion and sensor arrangements in ER-SG1 and ER-SG2.

Considering that the different outputs of HCF-SG from prior studies are not inferior compared with the reduction found in ur FE simulation, this implied that the hetero-core fiber on the gauge substrate could precisely respond to ΔD_s. Hence, as mentioned in the discussion of the FE analysis, the difference between the HCF-SG output and actual strain on the Al plate may be because the Al plate and the substrate curve locally at the vicinities of the two interfaces. Accordingly, for further precise strain measurement on a host structure, it is better to defuse the shear stress in the interface between the host structure and the substrate by inserting an adhesive sheet with a significantly lower Young's modulus than the host structure or by reducing the contact interface area.

IV. TEMPERATURE DEPENDENCE

Another experiment was conducted to evaluate the temperature dependency on the HCF-SG. As illustrated in Fig. 8, the HCF-SG and an electrical K-type thermocouple for reference were placed in a room at constant temperature. The HCF-SG was screwed on at one attachment point on a

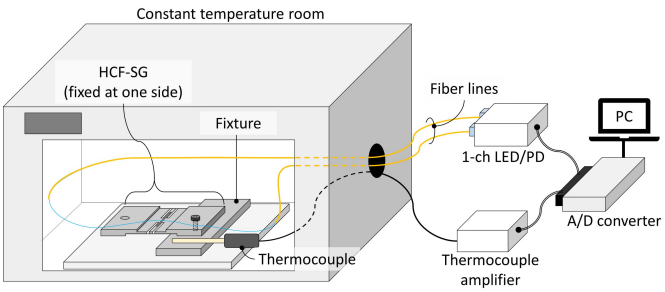

Fig. 8. Experimental setup for temperature dependency on the HCF-SG.

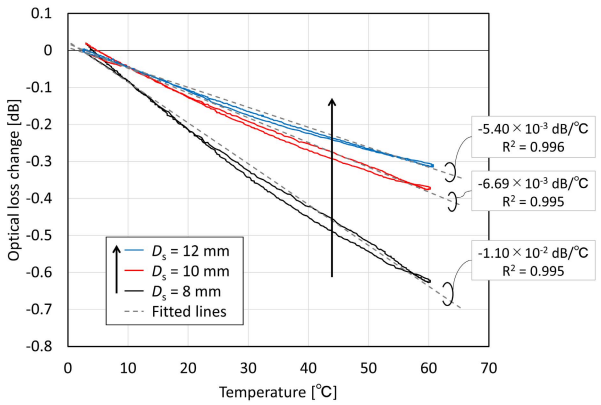

Fig. 9. Temperature dependency of the proposed HCF-SGs.

TABLE II
SENSITIVITY OF STRAIN AND TEMPERATURE FOR THE HCF-SGS

D_s [mm]	8	10	12
Strain coefficient (α_{str}) [dB/με]	-9.14 × 10^{-4}	-5.58 × 10^{-4}	-4.20 × 10^{-4}
Temp. coefficient (α_{tmp}) [dB/°C]	-1.10 × 10^{-2}	-6.69 × 10^{-3}	-5.40 × 10^{-3}
$\alpha_{tmp}/\alpha_{str}$ [με/°C]	12.0	11.9	12.9

fixture so that the gauge substrate would thermally expand with increase in room temperature. In this experiment, three HCF-SGs (D_s = 8, 10, 12 mm) were tested, and each HCF-SG and thermocouple were simultaneously monitored while the room temperature continuously changed from 0 °C to 60 °C from 60 °C to 0 °C.

Figure 9 shows the optical loss changes for the developed HCF-SGs in reaction to the room temperature monitored by the thermocouple. The optical loss changed owing to temperature variation from 0 °C to 60 °C, in which the temperature coefficient (α_{tmp}), which was approximated by linear fitting, decreased as D_s shortened. When comparing α_{tmp} to α_{str} in all cases of D_s, as shown in Table II, the ratio of α_{tmp} to α_{str} indicated 11.9-12.9 $\mu\epsilon$/°C with the same order of linear expansion coefficient for SUS304 (17.3 $\mu\epsilon$/°C). Actually, the temperature dependency of the sensors could be derived from multiple factors, such as the expansion and deflection of the gauge substrate mainly on the spring part, in addition to other thermal changes in the physical properties of the protective layer and epoxy adhesives covering the fiber line on the substrate. For instance, as shown in Fig. 9, the hysteresis observed in each sensor tends to increase with a smaller D_s. This is because the stress relaxation of the fiber beam shape becomes susceptible to the plasticity of the epoxy adhesive when the buckling stress of the fiber beam increases with a decreasing D_s value. However, the hysteresis also depends on the amount of adhesive; thus, it is actually difficult to control. To improve the sensor performance in terms of sensitivity and hysteresis, it is recommended that the hetero-core fiber is mechanically clamped on the gauge substrate at both sides of the spring part. Nevertheless, it was confirmed that the proposed HCF-SGs could measure temperature changes with a sensitivity that could be modulated by D_s, depending on the thermal expansion coefficient of the substrate.

V. CONCLUSION

This report described a novel optical strain gauge based on hetero-core fiber optics with a cost-effective measurement scheme and adjustable sensor performance. The hetero-core fiber optic sensor on the proposed strain gauge modulates the tensile and compression strain on the gauge substrate for the transmitted light loss. Because the slender structure of a fiber requires a considerably smaller stress to curve in Euler's buckling scheme compared to that of tensile stress, the mechanical properties of the strain gauge are less limited to those of the material that composes the fiber and can be tuned by the shape and material of the gauge substrate. We experimentally confirmed that the fiber sensor is capable of detecting $\mu\epsilon$-order strain by changing the dimensions of the displacement-to-bending converter mechanism with a strain sensitivity of up to -9.14×10^{-4} dB/$\mu\epsilon$ in the range of -3100 to 3100 $\mu\epsilon$. Additionally, the hetero-core fiber can linearly detect the displacement until fracture by excess bending so that the measurement range has a trade-off between strain sensitivity and can be expanded to ± 7140 $\mu\epsilon$ or more by increasing D_s above 12 mm. Moreover, through a series of anyalysis of the strain measurements on the Al base plate, the strain transfer mechanism from the host material to the gauge substrate reduced the measured strain by the HCF-SG to 0.81 times because of the stiffness of the substrate; thus, the mounting method and the substrate design can be further improved. The fabricated strain gauge was also confirmed to have temperature dependency mainly from the thermal expansion of the gauge substrate and D_s. Consequently, these results imply that the proposed hetero-core fiber optic strain gauge is applicable for strain measurements with tunable sensing performance, and it will be employed in future studies of multiple sensors to monitor stress, vibration, and temperature on SHM systems.

REFERENCES

[1] D. Logan and J. Mathew, "Using the correlation dimension for vibration fault diagnosis of rolling element bearings—I. Basic concepts," *Mech. Syst. Signal Process.*, vol. 10, no. 3, pp. 241–250, 1996.
[2] B.-S. Yang and K. J. Kim, "Application of Dempster–Shafer theory in fault diagnosis of induction motors using vibration and current signals," *Mech. Syst. Signal Process.*, vol. 20, no. 2, pp. 403–420, 2006.
[3] W. Fan and P. Qiao, "Vibration-based damage identification methods: A review and comparative study," *Struct. Health Monit., Int. J.*, vol. 10, no. 1, pp. 83–111, Jan. 2011.
[4] Y. An and J. Ou, "Experimental and numerical studies on model updating method of damage severity identification utilizing four cost functions," *Struct. Control Health Monitor.*, vol. 20, no. 1, pp. 107–120, Jan. 2013.

[5] H. Wang, P. Xiang, and L. Jiang, "Strain transfer theory of industrialized optical fiber-based sensors in civil engineering: A review on measurement accuracy, design and calibration," *Sens. Actuators A, Phys.*, vol. 285, pp. 414–426, Jan. 2019.
[6] T. Kissinger, E. Chehura, S. E. Staines, S. W. James, and R. P. Tatam, "Dynamic fiber-optic shape sensing using fiber segment interferometry," *J. Lightw. Technol.*, vol. 36, no. 4, pp. 917–925, Feb. 15, 2018.
[7] X. J. Yu, Y. L. Zhang, K. Li, J. T. Zhang, H. J. Lv, and S. C. Liu, "Frequency-division multiplexing sensing system based on multilongitudinal mode fiber lasers and beat frequency demodulation," *IEEE Photon. J.*, vol. 7, no. 2, Apr. 2015, Art. no. 7901307.
[8] T. Habisreuther, T. Elsmann, A. Graf, and M. A. Schmidt, "High-temperature strain sensing using sapphire fibers with inscribed first-order Bragg gratings," *IEEE Photon. J.*, vol. 8, no. 3, Jun. 2016, Art. no. 6802608.
[9] J. Ayers *et al.*, "Feasibility of component state awareness of high strain rate events using fiber Bragg grating sensors," *Int. J. Impact Eng.*, vol. 100, pp. 166–174, Feb. 2017.
[10] R. Li, Y. Chen, Y. Tan, Z. Zhou, T. Li, and J. Mao, "Sensitivity enhancement of FBG-based strain sensor," *Sensors*, vol. 18, no. 5, p. 1607, May 2018.
[11] X. Bai, D. Fan, S. Wang, S. Pu, and X. Zeng, "Strain sensor based on fiber ring cavity laser with photonic crystal fiber in-line Mach–Zehnder interferometer," *IEEE Photon. J.*, vol. 6, no. 4, Aug. 2014, Art. no. 6801608.
[12] R. Fan *et al.*, "Practical research on photonic crystal fiber micro-strain sensor," *Opt. Fiber Technol.*, vol. 52, Nov. 2019, Art. no. 101959.
[13] X. Dong, H. Du, X. Sun, Z. Luo, and J. Duan, "A novel strain sensor with large measurement range based on all fiber Mach–Zehnder interferometer," *Sensors*, vol. 18, no. 5, p. 1549, May 2018.
[14] Y. Ouyang *et al.*, "An in-fiber dual air-cavity Fabry–Perot interferometer for simultaneous measurement of strain and directional bend," *IEEE Sensors J.*, vol. 17, no. 11, pp. 3362–3366, Jun. 2017.
[15] G. Numata, N. Hayashi, M. Tabaru, Y. Mizuno, and K. Nakamura, "Ultra-sensitive strain and temperature sensing based on modal interference in perfluorinated polymer optical fibers," *IEEE Photon. J.*, vol. 6, no. 5, Oct. 2014, Art. no. 6802306.
[16] T. Geng *et al.*, "Modal interferometer using three-core fiber for simultaneous measurement strain and temperature," *IEEE Photon. J.*, vol. 8, no. 4, Aug. 2016, Art. no. 6803908.
[17] S. E. F. Masnan *et al.*, "Steel beam compressive strain sensor using single-mode-multimode-single-mode fiber structure," *IEEE Photon. J.*, vol. 8, no. 1, Feb. 2016, Art. no. 6801006.
[18] L. Ma, Y. Qi, Z. Kang, and S. Jian, "All-fiber strain and curvature sensor based on no-core fiber," *IEEE Sensors J.*, vol. 14, no. 5, pp. 1514–1517, May 2014.
[19] X. Jin *et al.*, "High strain sensitivity temperature sensor based on a secondary modulated tapered long period fiber grating," *IEEE Photon. J.*, vol. 11, no. 1, Feb. 2019, Art. no. 7100908.
[20] A. Leal-Junior *et al.*, "Characterization of a new polymer optical fiber with enhanced sensing capabilities using a Bragg grating," *Opt. Lett.*, vol. 43, no. 19, pp. 4799–4802, Oct. 2018.
[21] R. Ishikawa *et al.*, "Strain dependence of perfluorinated polymer optical fiber Bragg grating measured at different wavelengths," *Jpn. J. Appl. Phys.*, vol. 57, no. 3, Mar. 2018, Art. no. 038002.
[22] C. A. F. Marques *et al.*, "Fast and stable gratings inscription in POFs made of different materials with pulsed 248 nm KrF laser," *Opt. Express*, vol. 26, no. 2, pp. 2013–2022, Jan. 2018.
[23] R. Min *et al.*, "Microstructured PMMA POF chirped Bragg gratings for strain sensing," *Opt. Fiber Technol.*, vol. 45, pp. 330–335, Nov. 2018.
[24] I.-L. Bundalo, K. Nielsen, G. Woyessa, and O. Bang, "Long-term strain response of polymer optical fiber FBG sensors," *Opt. Mater. Express*, vol. 7, no. 3, pp. 967–976, 2017.
[25] K. Watanabe, K. Tajima, and Y. Kubota, "Macrobending characteristics of a hetero-core splice fiber optic sensor for displacement and liquid detection," *IEICE Trans. Electron.*, vol. 83, no. 3, pp. 309–314, Mar. 2000.
[26] H. Yamazaki, M. Nishiyama, K. Watanabe, and M. Sokolov, "Tactile sensing for object identification based on hetero-core fiber optics," *Sens. Actuators A, Phys.*, vol. 247, pp. 98–104, Aug. 2016.
[27] H. Yamazaki, I. Kurose, M. Nishiyama, and K. Watanabe, "Pendulum-type hetero-core fiber optic accelerometer for low-frequency vibration monitoring," *Sensors*, vol. 18, no. 8, p. 2528, Aug. 2018.
[28] H. Sasaki, Y. Kubota, and K. Watanabe, "Sensitivity property of a hetero-core-spliced fiber optic displacement sensor," *Proc. SPIE*, vol. 5579, pp. 136–143, Nov. 2004.
[29] C. H. Yoo and S. Lee, *Stability of Structures: Principles and Applications*. Amsterdam, The Netherlands: Elsevier, 2011.

Hiroshi Yamazaki received the B.E., M.E., and Ph.D. degrees in information systems science from Soka University, Tokyo, Japan, in 2013, 2015, and 2018, respectively. He has been an Assistant Professor with Soka University since 2018, working on development of fiber optic sensors.

Kazuhiro Watanabe received the B.E., M.E., and D.E. degrees in electrical engineering from Keio University, Yokohama, Japan, in 1976, 1978, and 1981, respectively. From April 1981 to March 1991, he was with the Department of Electrical Engineering, National Defense Academy, Yokosuka, Japan, where he was engaged in developments of high-power gas lasers. Since April 1991, he has been with the Faculty of Science and Engineering, Soka University, Tokyo, Japan, as a Professor. His current works are mainly in the fields of applications of fiber optic sensors and laser processing using femto-seconds, and short pulse lasers.